

Frequency independent quenching of pulsed emission

Vishal Gajjar

*National Centre for Radio Astrophysics (TIFR), Post Bag 3, Ganeshkhind, Pune - 411007 India;
Xinjiang Astronomical Observatory, Chinese Academy of Science, 40-5 South Beijing Road, Urumqi,
Xinjiang, 830011, China*

`gajjar@ncra.tifr.res.in`

Bhal Chandra Joshi

National Centre for Radio Astrophysics (TIFR), Post Bag 3, Ganeshkhind, Pune - 411007 India

`bcj@ncra.tifr.res.in`

Michael Kramer

*Max Planck Institute for Radio Astronomy Auf dem Hugel 69, P.O. Box 20 24, D-53010 Bonn, Germany;
Jodrell Bank Centre for Astrophysics, University of Manchester, Alan-Turing-Building, Manchester M13
9PL, UK*

`mkramer@mpifr-bonn.mpg.de`

Ramesh Karuppusamy

Max Planck Institute for Radio Astronomy Auf dem Hugel 69, P.O. Box 20 24, D-53010 Bonn, Germany

`ramesh@mpifr-bonn.mpg.de`

and

Roy Smits

*Jodrell Bank Centre for Astrophysics, School of Physics and Astronomy, University of Manchester,
Manchester M13 9PL, UK;*

Stichting ASTRON, Postbus 2, 7990 AA Dwingeloo, the Netherlands

`smits@astron.nl`

ABSTRACT

Simultaneous observations at four different frequencies *viz.* 313, 607, 1380 and 4850 MHz, for three pulsars, PSRs B0031–07, B0809+74 and B2319+60, are reported in this paper. Identified null and burst pulses are highly concurrent across more than decade of frequency. Small fraction of non-concurrent pulses ($\leq 3\%$) are observed, most of which occur at the transition instances. We report, with very high significance for the first time, full broadband nature of the nulling phenomenon in these three pulsars. These results suggest that nulling invokes changes on the global magnetospheric scale.

Subject headings: pulsars: general — pulsars: individual (PSR B0031–07, PSR B0809+74, PSR B2319+60)

1. Introduction

Pulsars show a variety of pulse to pulse variation in their pulsed emission. The most dramatic variation seen in many pulsars, with emission in a burst of one to several pulses interspersed with pulses with no detectable radio emission, is called pulse-nulling (Backer 1970). This phenomenon has been reported in more than 100 pulsars to date (Ritchings 1976; Rankin 1986; Biggs 1992; Vivekanand 1995; Wang et al. 2007; Gajjar et al. 2012). The pulsed emission abruptly declines by more than two orders of magnitudes during pulsar nulls (Lyne & Ashworth 1983; Vivekanand & Joshi 1997; Gajjar et al. 2012), which are as yet not well understood. Several sensitive studies of nulling pulsars have estimated the fraction of pulses with no detectable emission, called nulling fraction (NF). These range from less than a percent to about 90 percent (Ritchings 1976; Wang et al. 2007; Gajjar et al. 2014). Most of these studies were carried out at a single observing frequency with a typical observation length of about an hour. There are very few long simultaneous observations of nulling pulsars reported so far.

In a simultaneous single pulse study of two pulsars, PSRs B0329+54 and B1133+16 at 327 and 2695 MHz, Bartel & Sieber (1978) showed highly correlated pulse energy fluctuations, indirectly suggesting that nulling is a broadband phenomenon within this frequency range. However, only half of nulls were reported to occur simultaneously at 325, 610, 1400 and 4850 MHz for one of these pulsars, PSR B1133+16 (Bhat et al. 2007). Taylor et al. (1975) reported simultaneous nulls at 275 and 430 MHz for PSRs B0031-07 and B0809+74. Two separate studies on PSR B0809+74 reported contrary broadband nulling behavior. Bartel et al. (1981) reported concurrent nulling behavior at 102 and 1720 MHz for two long nulls while such concurrent behaviour was not apparent for three single period nulls, probably due to low signal-to-noise ratio (S/N). However, in simultaneous observations at 102 and 408 MHz, Davies et al. (1984) reported highly non-concurrent behavior, as only 3 out of 9 nulls were shown to be simultaneous.

There are two different group of theories that attempt to explain the cause of nulling. Intrinsic

effects such as cessation of primary particles on short time-scale Kramer et al. (2006), loss of coherence conditions (Filippenko & Radhakrishnan 1982; Zhang et al. 1997) or changes in the current flow (Timokhin 2010) may cause a pulsar to null. However, geometric effects such as line-of-sight passing between the emitting sub-beams producing the so-called *pseudo-nulls* (Herfindal & Rankin 2007, 2009; Rankin & Wright 2008) or changes in the direction of the entire emission beam (Arons 1983; Glendenning 1990; Dyks et al. 2005; Zhu & Xu 2006) can also mimic absence of detectable emission. As the emission at various radio frequencies is believed to originate at distinct heights from the neutron star surface (Komesaroff 1970; Cordes 1978; Mitra & Rankin 2002), the spacing between the sub-beam, in the rotating carousel, may also differ significantly from lower to higher frequencies (However, this needs to be confirmed firmly with more observations). Thus, the existence of *pseudo-nulls* (Herfindal & Rankin 2007) can be tested with simultaneous multiple frequency observations. Previously studied pulsars such as PSRs B0809+74 and B1133+16 represent a model of conal cut pulsar beam (Rankin & Ramachandran 2003; Rankin 1993), where it is difficult to distinguish between geometric and intrinsic effects. More long, sensitive, and simultaneous observations at multiple frequencies of a carefully selected sample of pulsars are motivated to distinguish between the above mentioned two groups of models.

In this paper, we report on long simultaneous multi-frequency observations of three pulsars, PSRs B0031-07, B0809+74 and B2319+60 to investigate the broadband nature of pulse nulling. These pulsars were chosen as (a) they are strong pulsars allowing an easy determination of nulls, (b) two of these pulsars, PSRs B0031-07 and B2319+60, show long prominent nulls (Huguenin et al. 1970; Ritchings 1976; Wright & Fowler 1981; Vivekanand 1995) and have high NF (40% and 30%), (c) two of these pulsars, PSRs B0031-07 and B0809+74, show prominent drifting and single component profile (Lyne & Ashworth 1983; Vivekanand & Joshi 1997) indicating a tangential and peripheral line-of-sight traverse of their emission beam, and (d) PSR B2319+60 shows a multiple component profile with drifting in outer components suggesting

a more central line of sight traverse of the emission beam (Rankin 1986; Wright & Fowler 1981; Gould & Lyne 1998). Thus, this sample allows us to test the effect of pulse nulling as a function of observational frequency for different parts of pulsar beam and discriminate between a geometric or an intrinsic origin for pulse nulling. In Section 2, observations and analysis procedures are described. The results are presented in Section 3. The conclusions of the study are presented in Section 4 along with a discussion on the implications of the results.

2. Observations and Analysis

PSRs B0031–07, B0809+74 and B2319+60 were observed simultaneously with the Giant Meterwave Radio Telescope (GMRT), the Westerbork Synthesis Radio telescope (WSRT) and the Effelsberg Radio Telescope. The details of observations are given in Table 1. The GMRT (Swarup et al. 1991) was used in a phased array mode with two sub-arrays consisting of about nine 45-m antennas each covering 313 and 607 MHz band respectively with 33-MHz bandwidth. The phased array output for each of the two frequencies were recorded with 512 channels over the passband using the GMRT software baseband receiver with an effective sampling time of 1 ms along with a time stamp for the first recorded sample, derived from a GPS disciplined Rb frequency standard. The variations in the ionospheric and instrumental delays across the GMRT sub-arrays have a typical time scale of about 2 hours at the observed frequencies. Hence, the observations were divided into 4 to 5 observing sessions, each of 2 hours, interspersed with compensation for the instrumental delay drift to maintain phasing of the sub-array.

The WSRT (Baars & Hooghoudt 1974) was also used in a tied array configuration of fourteen 25-m antennas covering 1380 MHz band with a 160-MHz bandwidth. The short spacing configuration of WSRT was employed to keep the ionospheric effects minimum. The 160-MHz radio frequency band, received with the Multi-Frequency Front-End (MFFE) at each antenna, were down-converted to an intermediate frequency (IF) and divided into eight 20-MHz subbands before digitization and addition in a tied array added mod-

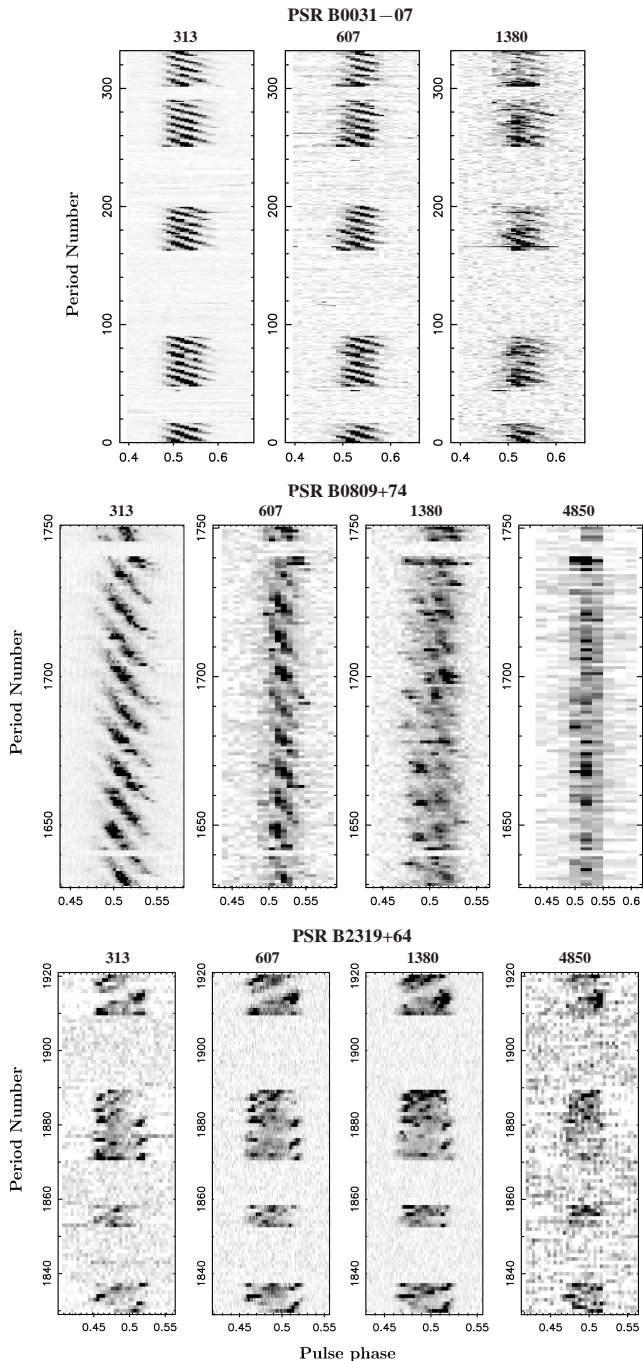


Fig. 1.— Single pulse sequence, with gray scaled intensity as a function of pulse number and pulse phase, for a subset of data at all frequencies for PSRs B0031–07, B0809+74 and B2319+60. The sequences were observed simultaneously at all frequencies. Concurrent occurrence of null pulses is clearly evident for each pulsar.

ule (TAAM). The data were acquired using an upgraded WSRT Pulsar Machine II (PuMa-II), which is a flexible cluster of 62 nodes capable of processing instantaneous observing bandwidth of 160 MHz (Karuppusamy et al. 2008). The data were recorded for each subband with a sampling time of 50 ns along with time-stamp derived from observatory’s Hydrogen maser for about 8 hours. The shorter baselines at WSRT together with its high latitude and higher observing frequency allows the tied array to remain phased for a longer time-scale than at lower frequencies used at the GMRT. Hence, a contiguous single pulse sequence was recorded at WSRT. The large data volume was reduced using off-line processing pipeline at WSRT to 8 dedispersed time-series with an effective sampling time of 1 ms.

The 100-m Effelsberg telescope was used at 4850 MHz with 500-MHz bandwidth in total intensity mode for two pulsars in the sample, PSRs B0809+74 and B2319+60. The detected signals from 6-cm dual horn secondary focus receiver were acquired using PSRFFTS search backend, configured to have 128 frequency channels across 500-MHz bandpass, with a dump time of 64 μ s and were recorded to a file along with a time-stamp derived from the observatory hydrogen maser.

Given the difference in the longitude of the observatories, the total overlap at all frequencies was smaller than the total duration of observations at each telescope. Part of the data during the overlap was affected by radio frequency interference (RFI) at one or the other telescope and was not considered for the analysis described below.

The data from all observatories were converted into a standard format required for SIGPROC¹ analysis package and dedispersed using the programs provided in the package. These were then folded to 1000 bins across the period using the ephemeris of these pulsars using TEMPO² package to obtain a single pulse sequence.

First, the pulse sequence for the longest data file, typically consisting of 6000 pulses, was averaged for each frequency to obtain an integrated profile, which was used to form a noise-free template, after centering the pulse, for the pulsar at that frequency. The template at each frequency

was used to estimate the number of samples to be removed from the beginning of each file for the observed frequencies so that the pulse is centered in a single period and time stamps for single pulses were corrected by these offsets. The single pulse sequences were then aligned by converting these time stamps to solar system barycentre (SSB) using TEMPO². This conversion also takes into account the delay at lower frequencies due to dispersion in the inter-stellar medium (ISM). Then, the pulses corresponding to identical time stamps at SSB across all frequencies were extracted from the data. It should be noted that, the ISM also introduces further delay to the propagating signal due to multi-path propagation, which is responsible for prominent pulse broadening at lower radio frequencies for high DM pulsars. The NE2001 electron density model (Cordes & Lazio 2002) predicts a delay of the order of 10^{-3} seconds for the highest DM pulsar in our sample. There is also a frequency dependent delay caused by the ionosphere which changes according to the time of the day. However, such delays are of the order of 10^{-7} seconds. Finally, there is a delay introduced by the Earth’s atmosphere, which is of the order of 10 ns [See Hobbs et al. (2006) for details of these delays]. For the current observations, where the comparison is carried out on the time-scale of the periods of the pulsars (~ 1 second), such delays can be ignored as they are three to seven orders of magnitude smaller, respectively. As the observations were typically recorded in 2–3 data files at the GMRT (313 and 607 MHz), the data recorded at WSRT and Effelsberg were split into similar number of files with observations duration equal to that at the GMRT.

The single pulse sequences were then visually examined to remove any single pulses with excessive RFI. The number of pulses available at all frequencies simultaneously after eliminating pulses affected by RFI are indicated in Table 1 for each pulsar. Nulling fractions (NFs) with their errors were obtained from the on-pulse energy and off-pulse energy sequences using a procedure similar to that described in Gajjar et al. (2012) for PSR B2319+60 and B0809+74. This method underestimates the NF for weaker pulsars with prominent sub-pulse drift as in the case of PSR B0031–07. Hence a method based on extreme values, described in Vivekanand (1995) was used for this

¹<http://sigproc.sourceforge.net/>

²<http://tempo.sourceforge.net/>

pulsar.

Sections of single pulse sequences with overlap on all frequencies and high S/N were extracted from the data as explained above. Null and burst pulses were identified using the threshold obtained from a histogram of on-pulse energy derived from on-pulse energy sequences, e.g. see Figure 1 in Gajjar et al. (2012). Any incorrectly identified null or burst pulse was relabeled after a careful visual examination of these plots to obtain a one-bit sequence with ones representing the bursts and zeros representing the nulls. Lengths of nulls (defined as a sequence of zeros bounded on both sides by bursts) and bursts were obtained for each frequency from the one-bit sequence and correlations between one-bit sequences across frequency were examined as explained in the next section.

3. Results

Single pulse sequences aligned in time across all frequencies for a section of data, observed simultaneously, are plotted for the three pulsars in Figure 1. All three pulsars show clear bursts interspersed with nulls. While PSRs B0031–07 and B2319+60 show frequent long nulls, PSR B0809+74 shows nulls up to 8 pulses separated by long sequence of burst pulses. Prominent drifting subpulses are seen in PSRs B0031–07 and B0809+74. The profiles of these pulsars (not shown) are known to evolve with frequency in a manner consistent with a tangential traverse of line-of-sight to the emission beam. For PSR B2319+60, subpulse drift has been reported at the edges of its profile (Wright & Fowler 1981). The multi-component nature of this pulsar’s profile implies a more central traverse of line-of-sight to the emission beam encompassing both the core and conal emission (Rankin 1986; Gould & Lyne 1998).

The pulsed emission switches simultaneously from burst state to null state (and vice versa) at all frequencies. This is true for both long nulls as well as short nulls (e.g. the null near pulse numbers 90 to 160 for PSR B0031–07 and 1638 to 1645 for PSR B0809+74 in Figure 1). A visual inspection of the entire data broadly confirms this behavior. The pulse energy in the bins, where pulsed emission is present is shown in Figure 2 for the three pulsars, suggesting similar correlated behavior across the frequencies. Thus by visually

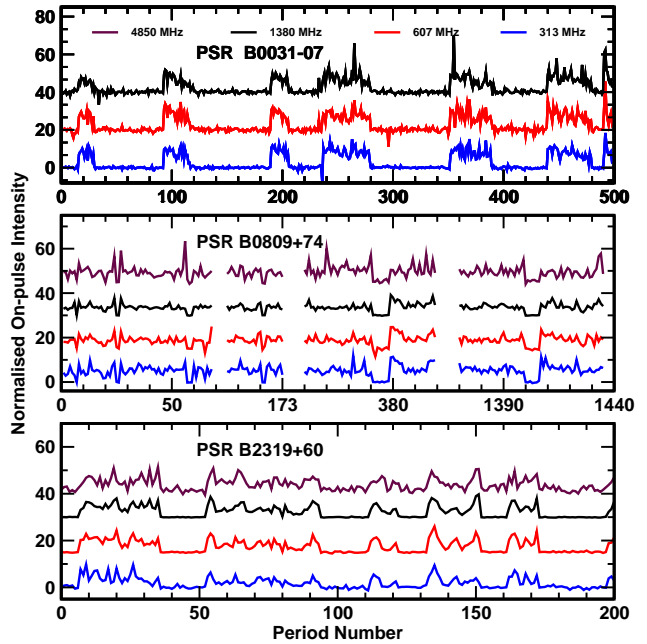


Fig. 2.— On-pulse energy sequences as a function of pulse number for a subset of data for all frequencies for PSRs B0031–07, B0809+74 and B2319+60. For B0809+74, four sections of single pulses exclusively around the null phases are shown.

inspecting the data, pulse nulling appears to be broadband over at least a decade of frequency for these pulsars.

The NF, the distributions of null and burst lengths and the correlation between the nulling pattern represented by the one-bit sequence were compared across frequencies to quantify this correlated behavior. The NFs estimated for the three pulsars were found to be consistent within errors across the observed frequencies (Table 2). The S/N was not sufficient to obtain a good estimate at 4850 MHz for PSR B0809+74 and B2319+60, so only a lower limit could be estimated in these cases. The combined NFs from all frequencies were estimated to be $42.8\% \pm 0.6\%$, $1.4\% \pm 0.2\%$ and $30.5\% \pm 0.6\%$ for PSRs B0031–07, B0809+74 and B2319+60, respectively. The expected error on the above mentioned NF was calculated as $1.9 \times \sqrt{NF(1-NF)/P}$, assuming binomial distribution of null pulses. It should be noted that, the NF is measured as a ratio of total number of null

pulses among P observed pulses combining all frequency data for each pulsar. These estimates are reported here to highlight the consistency with the previously reported NF values for these pulsars (Vivekanand 1995; Lyne & Ashworth 1983; Ritchings 1976).

The distributions of null and burst lengths, derived from the one-bit sequences, look similar for all frequencies for each pulsar indicating a very similar nulling pattern. These distributions were compared using a Kolmogorov-Smirnov test, which rejected, at a very high significance ($\geq 99.7\%$), the hypothesis that these distributions for any pair of frequencies are different.

Finally, the one-bit sequences for a pair of observing frequencies across all observations of each pulsar were compared using a contingency table analysis (Press et al. 1986). As these sequences represent two distinct states of a pulsar, the correlation between these states for a pair of frequency can be arranged as a 2×2 contingency table. A ϕ test (Cramer-V) and uncertainty test based on entropy calculations can then be used to assess the strength and significance of any correlation. Both these tests result in a value between 0 and 1. A value close to 1 indicates a strong correlation. Cramer's V for a 2×2 contingency table, as in our case, is just a measure of reduced chi-square. Hence, a value close to 1 indicates a very high significance of correlation. Likewise, a value close to unity for the uncertainty coefficient calculated from entropy arguments indicates a very high probability of observing null (burst) pulses at both frequencies. See Press et al. (1986) for details about these tests. The results of these tests are presented in Table 3. Both Cramer-V and the uncertainty coefficients have values very close to 1 for PSRs B0031–07 and B0809+74 indicating a significant high association across all pairs of frequencies. This is also the case for PSR B2319+60, although the strength is marginally smaller for association between pairs involving 4850 MHz.

For a small number of pulses, the above association does not hold. All such pulses were carefully examined for the three pulsars. About 44 pulses do not show simultaneous null (burst) state for PSR B0031–07. Among these, 25 occurred either at the start or at the end of a burst. There were 27 and 158 pulses observed in PSRs B0809+74 and B2319+60 respectively, where the state of pulse

was not identical across the frequencies. Similar to PSR B0031–07, 20 and 82 of these occurred at the start/end of a burst for PSRs B0809+74 and B2319+60, respectively. Thus, while the nulling patterns for the three pulsars is largely broadband, deviations from this behavior is seen in about one to three percent of pulses, about half of which occur at the transition from null to burst (or vice versa). The fraction of such pulses is marginally higher for PSR B2319+60 than that for PSRs B0031–07 and B0809+74. We did not find any correlation across frequencies in the number of these non-concurrent pulses as they appear to be similar for different pairs of frequencies for all three pulsars.

4. Discussion

We find that nulling is broadband for PSRs B0031–07, B0809+74 and B2319+60 with their NFs consistent across the frequencies. The distributions of null and burst pulses were found to be similar and the null-burst sequences show significantly high association from 313 to 4850 MHz. Deviation from this behavior was seen for less than 3% of the pulses, most of which occur at the transition state (from null to burst or vice versa). For PSR B0809+74, we found highly concurrent broadband behavior for both long and short nulls, contrary to the reported behavior by Bartel et al. (1981) and Davies et al. (1984). These studies were based on small number of pulses. It should be noted that our results are also different from those for PSR B1133+16, where 50% of null pulses were reported to be non-concurrent (Bhat et al. 2007). It is likely that B1133+16 exhibits unique frequency dependent nulling behavior while the pulsars studied here exhibit frequency independent quenching of pulsed emission. Another explanation could be the frequency dependent pulse-to-pulse modulation in PSR B1133+16. Bartel et al. (1980) suggested that pulse energy modulation decreases upto a critical frequency (~ 1 GHz) and then increases. This dependence of the pulse energy modulation may result in non-concurrent behavior in pulsars such as PSR B1133+16. Kramer et al. (2003) also speculated a loss in coherence across wide range of frequencies for this pulsar.

Among the two different group of theories,

geometric models invoking empty line-of-sight (*pseudo-nulls*) are unlikely to apply for these pulsars as the emission is expected to be seen at some frequency for higher number of instances due to the frequency dependent separation between sub-beams. For PSR B1133+16 also the emission seen at higher frequencies, during the nulls at lower frequencies, was shown to be distinct from the normal emission, probably originating at higher heights (Bhat et al. 2007). Moreover, as the sub-beams are arranged in a uniform pattern, unexcited emission regions imply some sort of periodicity, which is not seen in our data for these pulsars. Changes in emission geometry as in movement of emission region within the beam (Smits et al. 2005) also implies that the emission is expected to be seen at some frequency or other. While this is not ruled out, it is unlikely to be a general explanation for the nulling phenomenon considering that we do not see this emission for both conal pulsars such as PSRs B0031–07 and B0809+74 as well as for PSR B2319+60 which has a more central cut of the line of sight.

Intrinsic models invoking extinction of the sparking region or coherence conditions are consistent with our results. Such models propose the entire magnetosphere undergoing rapid changes to cause cessation of radio emission. Kramer et al. (2006) have shown cessation of emission to be associated with disruption of entire particle flow while Lyne et al. (2010) have shown radio emission changes (mode-changing) occurring on the global magnetospheric scale. Moreover, recent simultaneous observations of a mode-changing pulsar, PSR B0943+10, at radio and X-ray band also highlighted such global magnetospheric state switching (Hermsen et al. 2013). If the absence of emission during the null state is related to such intrinsic phenomena, the non-concurrent pulses may represent relaxation or local changes. The magnetospheric state switching may not be sudden and it is likely to possess finite relaxation time to switch between different states. For example, PSRs J1752+2359 and J1738–2330 show gradual decay and slow rise in the pulse energy before and after the null state respectively (Gajjar et al. 2014). This kind of gradual changes could manifest itself to give rise to differences in the emission state at different frequencies near the transition instances. Moreover, Bhat et al. (2007) also

reported lower frequencies to have longer nulls compared to nulls at higher frequencies in PSR B1133+16, pointing towards similar deviations at the transition instances. The distinct emission seen at higher frequencies for PSR B1133+16 can also be considered as a unique mode-changing phenomena in which one magnetospheric state does not produce detectable emission at lower frequencies. Thus, these results indicate that nulling seems to be another form of mode-change phenomena which invokes changes on the global magnetospheric scale, further supporting claims by Kramer et al. (2006) and Lyne et al. (2010).

We thank the staff of the GMRT who made these observations possible. The GMRT is operated by the National Centre for Radio Astrophysics of the Tata Institute of Fundamental Research (NCRA-TIFR). We would also like to thank staff of the WSRT and the Effelsberg radio telescope to make these simultaneous observations possible. VG acknowledge the West Light Foundation of the Chinese Academy of Sciences project XBBS-2014-21. We would also like to thank anonymous referee for the helpful comments.

REFERENCES

- Arons, J. 1983, in American Institute of Physics Conference Series, Vol. 101, Positron-Electron Pairs in Astrophysics, ed. M. L. Burns, A. K. Harding, & R. Ramaty, 163–193
- Baars, J. W. M., & Hooghoudt, B. G. 1974, *A&A*, 31, 323
- Backer, D. C. 1970, *Nat.*, 228, 42
- Bartel, N., & Sieber, W. 1978, *A&A*, 70, 307
- Bartel, N., Sieber, W., & Wolszczan, A. 1980, *A&A*, 90, 58
- Bartel, N., Kardashev, N. S., Kuzmin, A. D. Nikolaev, N. Y., et al. 1981, *A&A*, 93, 85
- Bhat, N. D. R., Gupta, Y., Kramer, M., et al. 2007, *A&A*, 462, 257
- Biggs, J. D. 1992, *ApJ*, 394, 574
- Cordes, J. M. 1978, *ApJ*, 222, 1006

- Cordes, J. M., & Lazio, T. J. W. 2002, ArXiv Astrophysics e-prints, arXiv:astro-ph/0207156
- Davies, J. G., Lyne, A. G., Smith, F. G., et al. 1984, MNRAS, 211, 57
- Dyks, J., Zhang, B., & Gil, J. 2005, ApJ, 626, L45
- Filippenko, A. V., & Radhakrishnan, V. 1982, ApJ, 263, 828
- Gajjar, V., Joshi, B. C., & Kramer, M. 2012, MNRAS, 424, 1197
- Gajjar, V., Joshi, B. C., & Wright, G. 2014, MNRAS, 439, 221
- Glendenning, N. K. 1990, ApJ, 359, 186
- Gould, D. M., & Lyne, A. G. 1998, MNRAS, 301, 235
- Herfidal, J. L., & Rankin, J. M. 2007, MNRAS, 380, 430
- . 2009, MNRAS, 393, 1391
- Hermesen et al. 2013, Science, 339, 436
- Hobbs et al. 2006, MNRAS, 369, 655
- Huguenin, G. R., Taylor, J. H., & Troland, T. H. 1970, ApJ, 162, 727
- Karuppusamy, R., Stappers, B., & van Straten, W. 2008, PASP, 120, 191
- Komesaroff, M. M. 1970, Nat., 225, 612
- Kramer, M., Karastergiou, A., Gupta, Y., et al. 2003, A&A, 407, 655
- Kramer, M., Lyne, A. G., O'Brien, J. T., Jordan, C. A., & Lorimer, D. R. 2006, Science, 312, 549
- Lyne, A. G., & Ashworth, M. 1983, MNRAS, 204, 519
- Lyne A., Hobbs G., Kramer M., Stairs I., Stappers B., 2010, Science, 329, 408
- Mitra, D., & Rankin, J. M. 2002, ApJ, 322
- Press, W. H., Flannery, B. P., Teukolsky, S. A., & Vetterling, W. T. 1986, Numerical Recipes: The Art of Scientific Computing (Cambridge: Cambridge University Press)
- Rankin, J. M. 1986, ApJ, 301, 901
- . 1993, ApJ, 405, 285
- Rankin, J. M., & Ramachandran, R. 2003, ApJ, 590, 411
- Rankin, J. M., & Wright, G. A. E. 2008, MNRAS, 385, 1923
- Ritchings, R. T. 1976, MNRAS, 176, 249
- Smits, J. M., Mitra, D., & Kuijpers, J. 2005, A&A, 440, 683
- Swarup, G., Ananthakrishnan, S., Kapahi, V. K., et al. 1991, Current Science, 60, 95
- Taylor, J. H., Manchester, R. N., & Huguenin, G. R. 1975, ApJ, 195, 513
- Timokhin, A. N. 2010, MNRAS, 408, L41
- Vivekanand, M. 1995, MNRAS, 274, 785
- Vivekanand, M., & Joshi, B. C. 1997, ApJ, 477, 431
- Wang, N., Manchester, R. N., & Johnston, S. 2007, MNRAS, 377, 1383
- Wright, G. A., & Fowler, L. A. 1981, A&A, 101, 356
- Zhang, B., Qiao, G. J., & Han, J. L. 1997, ApJ, 491, 891
- Zhu, W. W., & Xu, R. X. 2006, MNRAS, 365, L16

Table 1: Parameters of the observed pulsars and details of observations

Pulsar	Period	Dispersion Measure	Date of observations	Number of pulses	Frequencies of observations
	(s)	(pc cm ⁻³)			(MHz)
PSR B0031-07	0.942951	11.38	2011 February 5	10441	313, 607, 1380
PSR B0809+74	1.292241	6.12	2011 February 17	10003	313, 607, 1380, 4850
PSR B2319+60	2.256488	94.59	2011 February 6	5126	313, 607, 1380, 4850

Table 2: Estimated NFs of PSRs B0031-07, B0809+74 and B2319+60. Columns give pulsar name, number of pulses used in the analysis and NF at each of the indicated observing frequency

Pulsar	Number of pulses	Frequency of Observations (MHz)			
		303	607	1380	4850
PSR B0031-07	10441	43(2)	44(2)	43(2)	-
PSR B0809+74	10003	1.4(3)	1.6(4)	1.2(2)	> 1
PSR B2319+60	5126	35(5)	33(3)	31(2)	> 30

Table 3: Estimate of correlation significance and strength for one-bit sequences between a pair of frequencies for PSRs B0031-07, B0809+74 and B2319+60. The first row in each column for a given frequency gives the Cramer-V indicating the significance of correlation of one bit sequences associated with it and the frequency in the column. The second row in each column for a given frequency gives the corresponding uncertainty coefficient derived from entropy arguments (See Press et al. (1986))

Frequency of Observations (MHz)	PSR B0031-07		PSR B0809+74			PSR B2319+60		
	607	1380	607	1380	4850	607	1380	4850
313	0.99	0.99	0.96	0.97	0.96	0.98	0.98	0.94
	0.96	0.95	0.92	0.92	0.91	0.91	0.93	0.81
607	-	0.99	-	0.96	0.96	-	0.98	0.94
	-	0.94	-	0.91	0.90	-	0.94	0.83
1380		-		-	0.97		-	0.95
		-		-	0.92		-	0.85